IEEE Access
Multidisciplinary | Rapid Review | Open Access Journal

Received March 14, 2022, accepted March 29, 2022, date of publication April 4, 2022, date of current version April 8, 2022.

Digital Object Identifier 10.1109/ACCESS.2022.3164519

Sensorless Control Strategy of Permanent Magnet Synchronous Motor Based on Fuzzy Sliding Mode Observer

HONGCHANG DING, XINHONG ZOU, AND JINHONG LI
College of Mechanical and Electronic Engineering, Shandong University of Science and Technology, Qingdao 266590, China
Corresponding author: Hongchang Ding (dhchang@sdust.edu.cn)

ABSTRACT In this paper, a sensorless control strategy of permanent magnet synchronous motor (PMSM) based on fuzzy sliding mode observer (FSMO) is proposed. On the premise of satisfying the Lyapunov stability condition, a sliding mode observer (SMO) is constructed. The sigmoid function is used instead of the sign function as the switching function. The parameters of sigmoid function are adjusted in real time by establishing fuzzy rules to change the convergence characteristics of sigmoid function, so as to improve the observation performance. The back EMF signal extracted by the SMO can be made smoother by using the back EMF adaptive law, which reduces the chattering of the system and the observation error. In order to solve the problem that the traditional phase locked loop (PLL) can not be used when the positive and negative speed of the motor is switched, a tangent function PLL is proposed in this paper. Through the use of tangent function, the value and symbol of back EMF are avoided from entering the system, so as to realize the accurate estimation of rotor speed and rotor position under the condition of positive and negative speed switching. The designed Fuzzy Sliding Mode Observer is simulated in Matlab/Simulink, and the experimental verification is carried out on the 2kW surface mounted PMSM vector control platform with TMS320F28335 as the main control chip. Simulation and experimental results show that this method can effectively track the changes of rotor speed and position when the motor is switched between positive and negative speed, and has the characteristics of fast convergence, small chattering and good robustness.

INDEX TERMS Permanent magnet synchronous motor, sensorless control, fuzzy sliding mode observer, back EMF adaptive law, tangent function phase locked loop.

I. INTRODUCTION

PMSMs have many advantages, such as high power density, wide speed range and fast dynamic response, and are widely used in servo drives, electric vehicles and other fields. When using field-oriented vector control, in order to make the PMSM control system have higher performance, it is necessary to obtain accurate information of the motor speed and rotor position. The traditional method is to install mechanical sensors in the system, but the usage of mechanical sensors will increase the instability of the system and the cost. In order to solve this problem, a position sensorless control method is proposed. The current position sensorless control methods are mainly divided into two categories: one is the high-frequency signal injection method, which is suitable for the situation where the motor is running at zero and low speed. By injecting high-frequency signals into the motor, and extracting high-frequency signals to obtain the rotor position and speed information of the motor [1], [2]. The other is the method based on the fundamental wave mathematical model, which is suitable for the motor running at medium and high speed. It mainly includes extended Kalman filter algorithm, model reference adaptive control algorithm, SMO algorithm and so on. The extended Kalman filter algorithm has the advantages of good dynamic performance and high observation accuracy. However, the extended Kalman filter method has a complex structure, a large amount of calculation, and a high requirement for a digital processor, which limits the application of this method in motor control systems [3], [4]. Model reference adaptive control algorithm is widely used in the identification of motor parameters, motor speed and rotor position of motors. Its structure is simple and easy to implement digitally, but the estimation accuracy of this method has a high dependence on system parameters [5]–[8].

The associate editor coordinating the review of this manuscript and approving it for publication was Dong Shen.

Compared with other algorithms, the SMO algorithm has the advantages of strong robustness when external disturbance or parameter changes and simple calculation. However, the chattering problem in the algorithm of SMO is inevitable due to the switching function [9], [10]. Therefore, how to suppress chattering is the key to the improvement of SMO.

The sliding mode variable structure control theory was first proposed in the 1950s [11]. This is a special nonlinear control, so its control system is discontinuous. The structure of the entire control system changes with the change of the switching characteristics rather than being fixed. Switch conversion makes the structure of the control system in a dynamic jump process. According to this principle, the difference between the input variable of the system and the given variable is used as the basis for judging the switch control characteristics, forcing the system to move according to the artificially set sliding mode. And the motion equation of the sliding mode only depends on the selected switching function, and has nothing to do with the system [12], [13]. The SMO algorithm is proposed based on the principle of sliding mode variable structure. SMO inherits the advantages of sliding mode variable structure control, such as the uncertainty of system modeling and strong robustness to external disturbances, and the dynamic characteristics of SMO are only determined by the selected switching function. The SMO method is widely used in medium and high speed sensorless PMSM vector control systems [14]–[16].

Determined by the sliding mode variable structure control principle, high frequency chattering is unavoidable in the SMO. The traditional method is to use a low-pass filter to suppress chattering in the SMO [17], [18]. However, the use of low-pass filters will produce phase lag. Therefore, a phase compensation module needs to be added to the system. The phase compensation module needs to use the arctan function and the estimated speed, which will further increase the estimated error of the rotor position and speed. An adaptive SMO with good robustness to parameter disturbance is proposed in references [14], [19], [20]. In reference [21], the saturation function is used as the switching function, and the chattering is reduced by designing a reasonable boundary layer thickness, however, because the transition of the saturation function curve at the boundary layer is not smooth, this method will still produce a small amount of chattering. In reference [22], the sigmoid function is used instead of the sign function, which plays a certain role in weakening the high frequency chattering of the back EMF signal. A fuzzy SMO is proposed in references [23]–[25], the fuzzy logic control is used to adjust the switching gain of the SMO, which can weaken the chattering of the motor at low speed. A second-order sliding mode algorithm based on superhelix is proposed in references [26]–[28], the chattering of the system is reduced by the combination of superhelix algorithm and SMO algorithm. In references [29], [30], the neural network is applied to the SMO to obtain the switching gain, which can reduce chattering, but it will increase the complexity of the system. A compound sliding mode control method based on a new hybrid reaching law with disturbance compensation is proposed in reference [31], which can compensate the external disturbance.

In this paper, a FSMO is proposed to extract rotor speed and rotor position information. The back EMF adaptive law is used to process the back EMF signal to reduce the system chattering and improve the observation performance of the SMO. The tangent function PLL is used to observe the rotor speed and rotor position when the positive and negative speed of the motor is switched. This paper is mainly divided into the following parts: The first section is the introduction. In the second section, the improved SMO is designed. In the third section, the tangent function PLL is proposed, and its effect is compared with the traditional PLL. In the fourth and fifth sections, the proposed algorithm is verified by simulation and experiment. The last section summarizes the research of the article and draws conclusions.

II. DESIGN OF SMO

A. MATHEMATICAL MODEL OF PMSM

The stator voltage state equation of the surface mount PMSM in the $\alpha - \beta$ coordinate system is:

$$\begin{bmatrix} u_\alpha \\ u_\beta \end{bmatrix} = \begin{bmatrix} R + pL_s & \\ & R + pL_s \end{bmatrix} \begin{bmatrix} i_\alpha \\ i_\beta \end{bmatrix} + \begin{bmatrix} E_\alpha \\ E_\beta \end{bmatrix} \tag{1}$$

where L_s is the stator inductance; $p = \frac{d}{dt}$ is the differential operator; $\begin{bmatrix} E_\alpha & E_\beta \end{bmatrix}^T$ is the extended back EMF; $\begin{bmatrix} u_\alpha & u_\beta \end{bmatrix}^T$ is the stator voltage; $\begin{bmatrix} i_\alpha & i_\beta \end{bmatrix}^T$ is the stator current.

The extended back EMF expression is:

$$\begin{bmatrix} E_\alpha \\ E_\beta \end{bmatrix} = \omega_e \psi_f \begin{bmatrix} -\sin\theta_e \\ \cos\theta_e \end{bmatrix} \tag{2}$$

In Eq. (2), θ_e is the electrical angle; ψ_f is the permanent magnet flux linkage, ω_e is the electrical angular velocity.

From Eq. (2), it can be seen that the back EMF of the surface-mount PMSM is related to the speed of the motor and the position of the rotor. The greater the back EMF, the greater the motor speed. Therefore, the speed and rotor position information of the motor can be obtained from the back EMF signal of the motor.

B. TRADITIONAL SMO

Rewrite the voltage equation of Eq. (1) into the state equation of current:

$$\frac{d}{dt}\begin{bmatrix} i_\alpha \\ i_\beta \end{bmatrix} = -\frac{R}{L_s}\begin{bmatrix} i_\alpha \\ i_\beta \end{bmatrix} + \frac{1}{L_s}\begin{bmatrix} u_\alpha \\ u_\beta \end{bmatrix} - \frac{1}{L_s}\begin{bmatrix} E_\alpha \\ E_\beta \end{bmatrix} \tag{3}$$

In the SMO, the sign function is used as the switching function. Due to the discontinuity of the sign function, the system is easy to produce chattering during operation. In this paper, the continuous sigmoid function is used to replace the sign function. The definition formula of sigmoid function is Eq. (4).

$$sigmoid(s) = \frac{2}{1 + e^{-as}} - 1 \tag{4}$$

where a is a positive constant, and its size affects the convergence characteristics of the function. The sigmoid curve is shown in Fig. 1. It can be seen from Fig. 1 that when the value of a is larger, the convergence speed of sigmoid function is faster, but it will produce larger chattering. When the value of a is small, although the system chattering is small, it will slow down the speed of the system approaching the sliding mode surface. Therefore, it is necessary to select an appropriate value of a to ensure faster convergence speed and less chattering of the system.

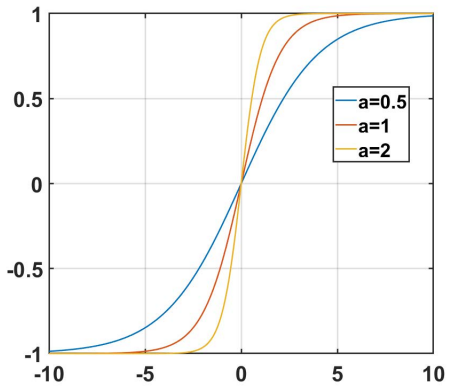

FIGURE 1. Curve of sigmoid function.

In order to design the SMO, the sliding mode surface function is defined:

$$S = \begin{bmatrix} \tilde{i}_\alpha \\ \tilde{i}_\beta \end{bmatrix} = \begin{bmatrix} \hat{i}_\alpha - i_\alpha \\ \hat{i}_\beta - i_\beta \end{bmatrix} \tag{5}$$

According to Eq. (3) and Eq. (5), the SMO can be constructed as:

$$\frac{d}{dt}\begin{bmatrix} \hat{i}_\alpha \\ \hat{i}_\beta \end{bmatrix} = -\frac{R}{L_s}\begin{bmatrix} \hat{i}_\alpha \\ \hat{i}_\beta \end{bmatrix} + \frac{1}{L_s}\begin{bmatrix} u_\alpha \\ u_\beta \end{bmatrix} - \frac{1}{L_s}\begin{bmatrix} \hat{E}_\alpha \\ \hat{E}_\beta \end{bmatrix} + k\begin{bmatrix} sigmoid(\tilde{i}_\alpha) \\ sigmoid(\tilde{i}_\beta) \end{bmatrix} \tag{6}$$

where $\hat{i}_\alpha$ and $\hat{i}_\beta$ are estimated current values. $\tilde{i}_\alpha = \hat{i}_\alpha - i_\alpha$ and $\tilde{i}_\beta = \hat{i}_\beta - i_\beta$ are the current estimation errors. k is a positive constant. $\hat{E}_\alpha = -\hat{\omega}_e\psi_f \sin\hat{\theta}_e$ and $\hat{E}_\beta = \hat{\omega}_e\psi_f \cos\hat{\theta}_e$ are the estimated back EMF of the motor. $\tilde{E}_\alpha = \hat{E}_\alpha - E_\alpha$ and $\tilde{E}_\beta = \hat{E}_\beta - E_\beta$ are the estimation errors of back EMF. $\hat{\theta}_e$ and $\hat{\omega}_e$ are the estimated values of the rotor position and speed of the motor, respectively.

Subtracting Eq. (3) from Eq. (6), the stator current error equation can be obtained:

$$\frac{d}{dt}\begin{bmatrix} \tilde{i}_\alpha \\ \tilde{i}_\beta \end{bmatrix} = -\frac{R}{L_s}\begin{bmatrix} \tilde{i}_\alpha \\ \tilde{i}_\beta \end{bmatrix} - \frac{1}{L_s}\begin{bmatrix} \tilde{E}_\alpha \\ \tilde{E}_\beta \end{bmatrix} + k\begin{bmatrix} sigmoid(\tilde{i}_\alpha) \\ sigmoid(\tilde{i}_\beta) \end{bmatrix} \tag{7}$$

When the system reaches the sliding surface, Eq. (8) holds.

$$S = \dot{S} = 0 \tag{8}$$

From Eq. (8) and Eq. (7), the estimated back EMF is:

$$\begin{bmatrix} \tilde{E}_\alpha \\ \tilde{E}_\beta \end{bmatrix} = kL_s\begin{bmatrix} sigmoid(\tilde{i}_\alpha) \\ sigmoid(\tilde{i}_\beta) \end{bmatrix} \tag{9}$$

In this paper, Lyapunov theorem is used to judge the stability of SMO. The form of Lyapunov function is as follows:

$$V = \frac{1}{2}S^T S = \frac{1}{2}\tilde{i}_\alpha^2 + \frac{1}{2}\tilde{i}_\beta^2 \tag{10}$$

The derivative of Lyapunov function can be obtained:

$$\dot{V} = \tilde{i}_\alpha\frac{d}{dt}\tilde{i}_\alpha + \tilde{i}_\beta\frac{d}{dt}\tilde{i}_\beta \tag{11}$$

Substituting Eq. (7) into Eq. (11), we can get

$$\dot{V} = -\frac{R}{L_s}\left(\tilde{i}_\alpha^2 + \tilde{i}_\beta^2\right) - \frac{\tilde{i}_\alpha}{L_s}\left(ksigmoid\left(\tilde{i}_\alpha\right) - E_\alpha\right) - \frac{\tilde{i}_\beta}{L_s}\left(ksigmoid\left(\tilde{i}_\beta\right) - E_\beta\right) \tag{12}$$

When $\dot{V} < 0$, the SMO is stable. Therefore, the value of k can be obtained when the SMO is stable.

$$k > \max\left(|E_\alpha|, |E_\beta|\right) \tag{13}$$

C. FSMO

In order to reduce chattering and improve the observation performance of SMO. Fuzzy rules are established to adaptively adjust the value of parameter a in sigmoid function. When the motion point of the system is far from the sliding mode surface, it increases the value of a, so that the system quickly approaches the sliding mode surface. When the moving point of the system is closely to the sliding mode surface, it reduces the value of a, which will reduce the chattering of the system.

Fuzzy control is an intelligent control method based on fuzzy rule table, which is based on fuzzy set. Fuzzy control mainly includes three steps: fuzzification, fuzzy inference and defuzzification. In this paper, the input variables s and $\dot{s}$ are fuzzified by fuzzy set {NB, NM, NS, ZO, PS, PM, PB}. The fuzzy set used for output variable a is {ZO, PS, PM, PB}. Among them: N = Negative, B = Big, M = Middle, S = Small, ZO = Zero, P = Positive. The membership functions of all parameters are trigonometric functions. Mamdani method is used as fuzzy inference algorithm. The center of gravity method is used to defuzzify the output variables. Table 1 shows the fuzzy rules established in this paper. Fig. 2 shows the membership function of variables s and $\dot{s}$. Fig. 3 shows the membership function of variable a.

D. THE DESIGN OF BACK EMF ADAPTIVE LAW

In order to further filter the noise and harmonics in the back EMF signal and obtain a smoother back EMF signal, an adaptive parameter l is introduced in this paper to design the back EMF adaptive law. By selecting the appropriate value of l, a smoother back EMF signal can be obtained, thereby obtaining more accurate speed and rotor position information, and improving the observation performance of the SMO.

TABLE 1. Fuzzy rules.

$\dot{s}$ \ a	NB	NM	NS	ZO	PS	PM	PB
NB	PB	PB	PB	PB	PB	PB	PB
NM	PB	PB	PM	PM	PM	PB	PB
NS	PB	PM	PS	PS	PS	PM	PB
ZO	PB	PM	PS	ZO	PS	PM	PB
PS	PB	PM	PS	PS	PS	PM	PB
PM	PB	PB	PM	PM	PM	PB	PB
PB	PB	PB	PB	PB	PB	PB	PB

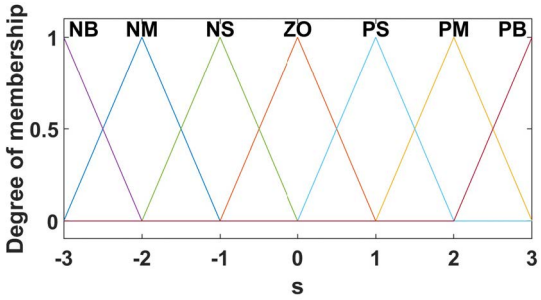

FIGURE 2. The membership function diagram of variable s ($\dot{s}$).

The back EMF adaptive law can be designed as:

$$\begin{cases} \frac{d}{dt}\tilde{E}_\alpha = -\hat{\omega}_e\hat{E}_\beta + \omega_e E_\beta - l\tilde{E}_\alpha \\ \frac{d}{dt}\tilde{E}_\beta = -\hat{\omega}_e\hat{E}_\alpha + \omega_e E_\alpha - l\tilde{E}_\beta \\ \frac{d}{dt}\tilde{\omega}_e = \tilde{E}_\alpha\hat{E}_\beta - \hat{E}_\alpha\tilde{E}_\beta \end{cases} \tag{14}$$

where l is a positive constant. If the value of l is too small, it will cause distortion of the back EMF waveform estimated by the SMO, and cause greater chattering in the control system. When the value of l is too large, the response time of the system will increase, which will affect the dynamic performance of the system.

III. THE DESIGN OF PLL

A. TRADITIONAL PLL

In the traditional method, the rotor position of the motor is obtained by arctan.

$$\hat{\theta} = -\arctan\left(\frac{\hat{E}_\alpha}{\hat{E}_\beta}\right) \tag{15}$$

However, due to the switching characteristics of sliding mode control, high-frequency chattering is inevitable when the system moves on the sliding mode surface. Therefore, there will be high-frequency chattering in the observed back EMF signal. If the arctan function is used to calculate the rotor position, because of the existence of the division in the arctan function, the high-frequency chattering in the back EMF signal will be amplified, resulting in a larger error in the rotor position. In order to solve this problem, a PLL is generally used to extract the rotor position information from the back EMF signal.

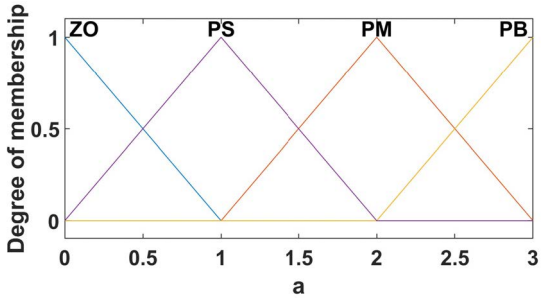

FIGURE 3. The membership function diagram of variable a.

The block diagram of traditional PLL is shown as in Fig. 4. K_p and K_i are the proportional gain and integral gain in the PLL. The estimated error of the rotor position can be expressed as:

$$\varepsilon(t) \propto \left(\sin\theta_e\cos\hat{\theta}_e - \cos\theta_e\sin\hat{\theta}_e\right) \propto \sin\left(\theta_e - \hat{\theta}_e\right) \tag{16}$$

When $\left|\theta_e - \hat{\theta}_e\right| < \frac{\pi}{6}$, it can be considered that $\sin\left(\theta_e - \hat{\theta}_e\right) = \theta_e - \hat{\theta}_e$ is valid.

$$\varepsilon\,(t) \propto \theta_e - \hat{\theta}_e \tag{17}$$

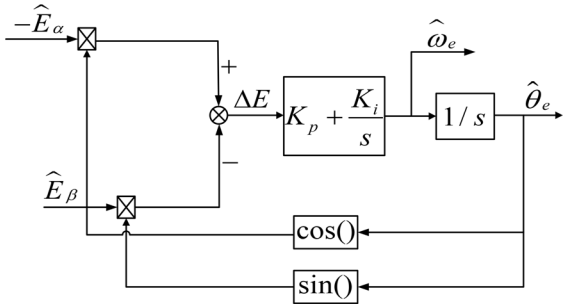

FIGURE 4. Block diagram of a traditional PLL.

Assuming that the operating frequency of the PLL is much higher than its input update frequency, when the motor speed is forward, the nonlinear dynamic equation of the PLL system can be expressed as:

$$\begin{cases} \dot{e_\theta} = e_\omega \\ \dot{e_\omega} = -K_p E\cos(e_\theta)\,e_\omega - K_i E\sin(e_\theta) \end{cases} \tag{18}$$

where $e_\theta = \theta_e - \hat{\theta}_e$, $e_\omega = \omega_e - \hat{\omega}_e$, $E = \hat{\omega}_e\psi_f$.

However, when the motor reverses, that is, when the motor speed is negative, $\omega_e \to -\omega_e$ will cause $\varepsilon \to -\varepsilon$. If the values of K_p and K_i remain unchanged, the nonlinear dynamic equation of the PLL system is:

$$\begin{cases} \dot{e_\theta} = e_\omega \\ \dot{e_\omega} = K_p|E|\cos(e_\theta)\,e_\omega + K_i|E|\sin(e_\theta) \end{cases} \tag{19}$$

The nonlinear dynamic equations of the traditional PLL are different when the motor rotates forward and reverse. Therefore, the traditional PLL cannot be used in the control system of the motor forward and reverse switching. When the proportional gain and integral gain of the PI regulator are

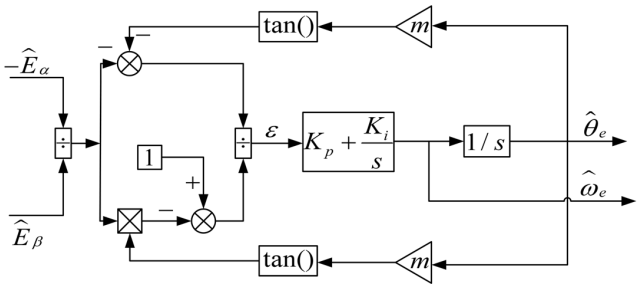

FIGURE 5. Structure diagram of tangent function PLL.

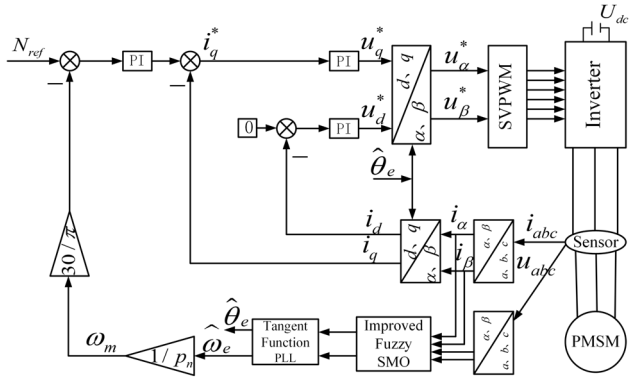

FIGURE 6. Block diagram of sensorless control system of PMSM.

TABLE 2. Simulation parameter settings.

Parameter	Value
Parameter in adaptive law l	60000
SMO gain value k	10000
Proportional coefficient K_p	129000
Integral coefficient K_i	586000

determined, the traditional PLL can only be used at the same direction of rotation. When the speed direction is switched, a rotor position error of 180° will be generated. To solve this problem, the value of the PI regulator can be used as the gain value of the estimated speed sign function for adjustment. But this method is not easy to implement in the actual system. Therefore, the traditional PLL cannot be applied to the situation where the motor is switched between positive and negative speeds [32], [33].

B. IMPROVED PLL

Because it will be affected by the positive and negative speed directions, the use of traditional PLL for rotor position estimation will have large estimation errors. This paper designs a PLL based on the tangent function to replace the traditional PLL to solve this problem. The main principle is to prevent the value and sign of E from entering the system through the tangent function. Fig. 5 is a structural diagram of the tangent function PLL.

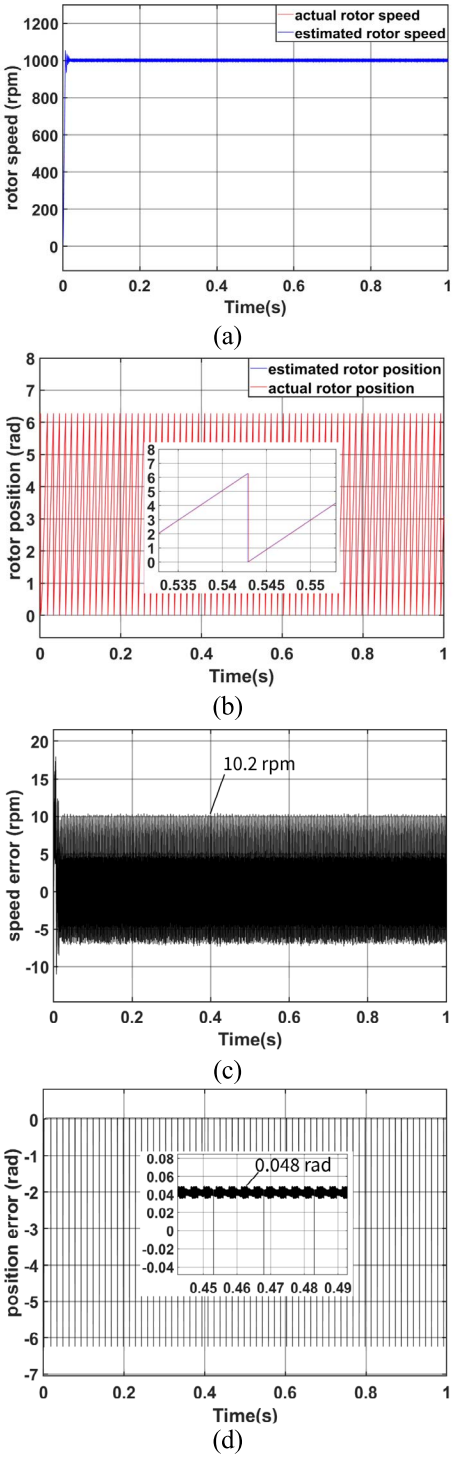

FIGURE 7. Simulation results of traditional SMO. (a) Rotor speed. (b) Rotor position. (c) Rotor speed error. (d) Rotor position error.

$\varepsilon(t)$ is derived from the form of the tangent function:

$$\varepsilon(t) = \frac{\tan\theta_e - \tan(m\hat{\theta}_e)}{1 + \tan\theta_e \tan(m\hat{\theta}_e)} = \tan(\theta_e - m\hat{\theta}_e) \tag{20}$$

where m is a positive constant, and $m = \frac{1}{2}$ is taken here. Compared with the traditional PLL, the PLL based on the tangent function eliminates the E in the error $\varepsilon(t)$, and the

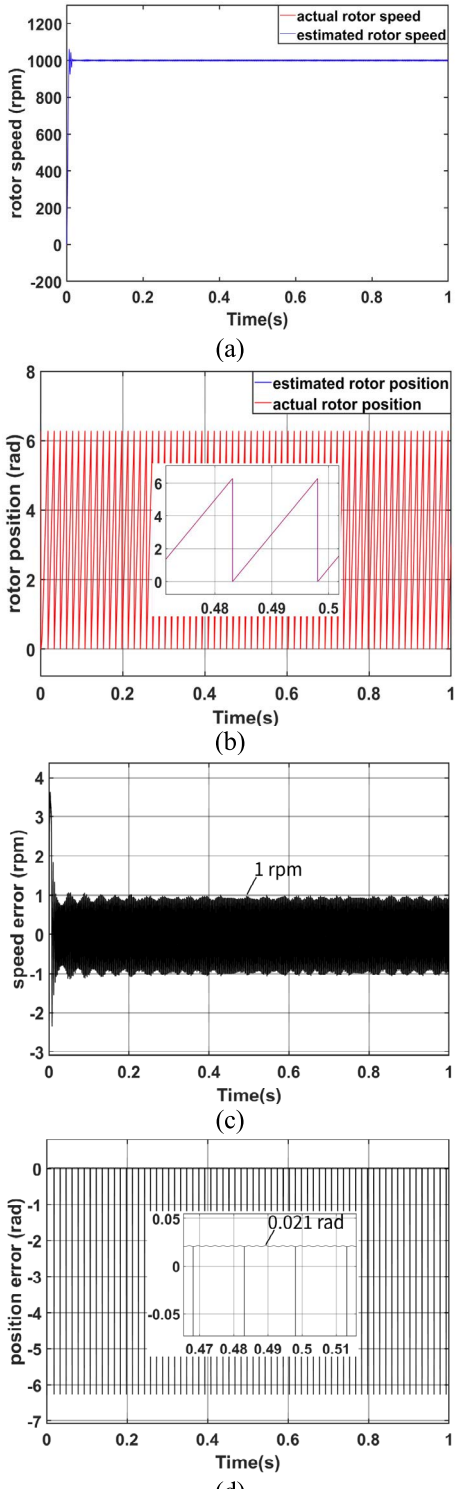

FIGURE 8. Simulation results of the improved SMO. (a) Rotor speed. (b) Rotor position. (c) Rotor speed error. (d) Rotor position error.

sign of $\varepsilon(t)$ will not change when the motor rotation direction changes. Therefore, the parameters of the PI regulator determined in the case of the motor rotating forward are also applicable to the case of the motor rotating in the reverse direction.

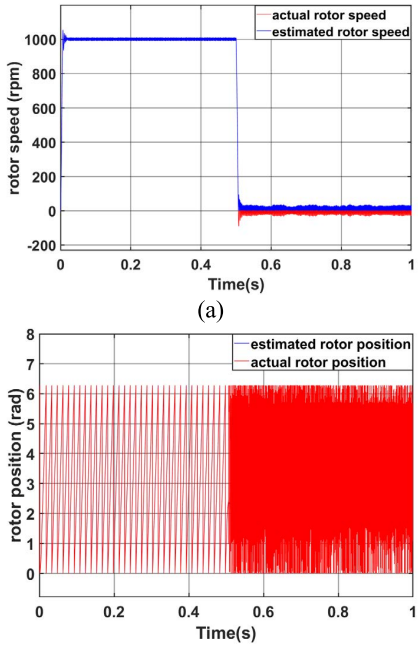

FIGURE 9. Simulation results of traditional SMO + traditional PLL during positive and negative speed switching of motor. (a) Rotor speed. (b) rotor position.

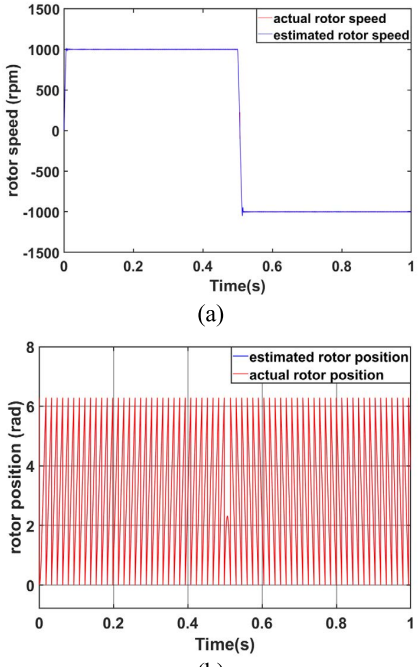

FIGURE 10. Simulation results of improved SMO + tangent function PLL during positive and negative speed switching of motor. (a) Rotor speed. (b) rotor position.

The nonlinear error dynamic equation of the PLL system based on the tangent function can be derived as:

$$\begin{cases} \dot{e_\theta} = e_\omega \\ \dot{e_\omega} = -mK_p \dfrac{1}{\cos^2(e_\theta)} e_\omega - mK_i \tan(e_\theta) \end{cases} \tag{21}$$

where $e_\theta = \theta_e - m\hat{\theta}_e$ and $e_\omega = \omega_e - m\hat{\omega}_e$.

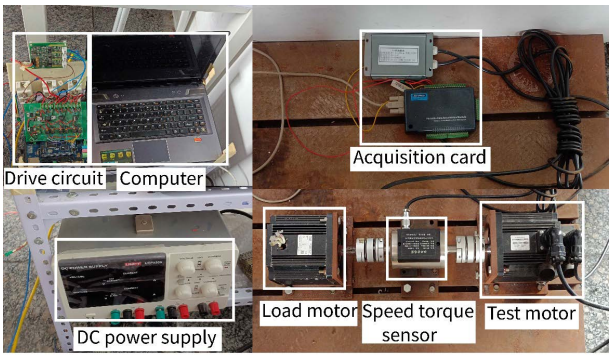

FIGURE 11. Experimental platform.

TABLE 3. Motor parameters.

Parameters	Units	Values
Rated power	kW	2.0
Rated current	A	7.5
Rated voltage	V	220
Rated torque	N·m	7.7
PWM switching frequency	kHz	10
Flux linkage	Wb	0.0588
Stator resistance	Ω	1.575
Stator inductance	mH	2.94
Pole pair		4
Inertia	kg·m^2	0.002017
DC side voltage	V	311

The transfer function of the tangent function PLL can be derived as:

$$G_{PLL} = \frac{\hat{\theta}_e}{\theta_e} = \frac{K_p s + K_i}{s^2 + mK_p s + mK_i} \tag{22}$$

IV. ANALYSIS OF SIMULATION RESULTS

In order to verify the reliability and effectiveness of the PMSM sensorless control strategy based on FSMO proposed in this paper, simulations were carried out in Matlab/Simulink, and the block diagram is established as shown in Fig. 6. The method of vector control is adopted. The modulation method of PWM is space vector pulse width modulation. Both the current loop and the speed loop use PI regulators. The processing method of back EMF is to use an improved SMO method to extract the positive sequence component of back EMF. A PLL based on tangent function is used to extract position information instead of the traditional PLL. The simulation parameter settings are shown in Table 2, and the motor parameters are shown in Table 3.

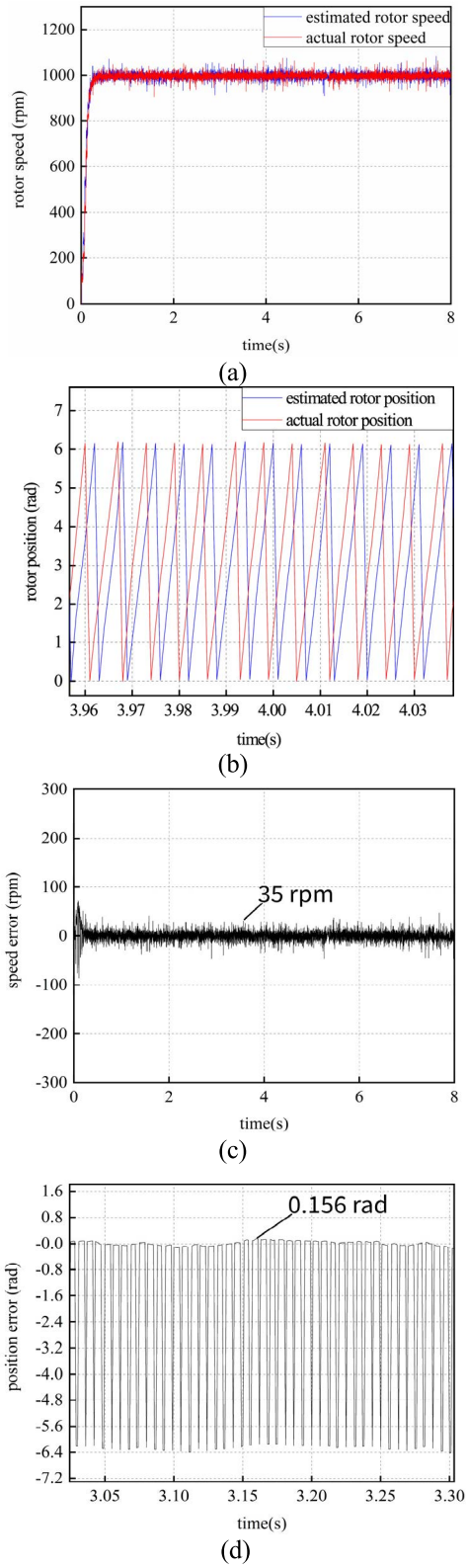

FIGURE 12. Experimental results of traditional SMO. Rotor speed. (b) Rotor position. (c) Rotor speed error. (d) Rotor position error.

Fig. 7 shows the simulation results of the traditional SMO. Fig. 8 shows the simulation results of the improved SMO. Table 4 shows the comparison of the simulation results of

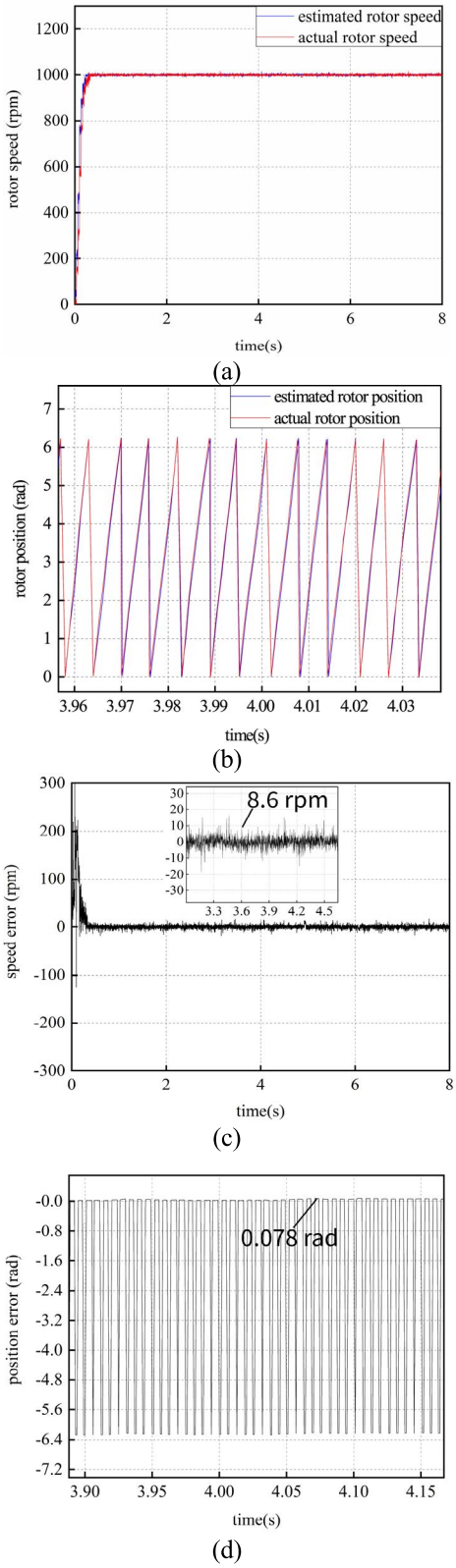

FIGURE 13. Experimental results of an improved SMO. (a) Rotor speed. (b) Rotor position. (c) Rotor speed error. (d) Rotor position error.

the two control methods. The motor starts at no load and then runs at 1000 rpm. It can be seen from the simulation results that the maximum steady-state error of the rotational

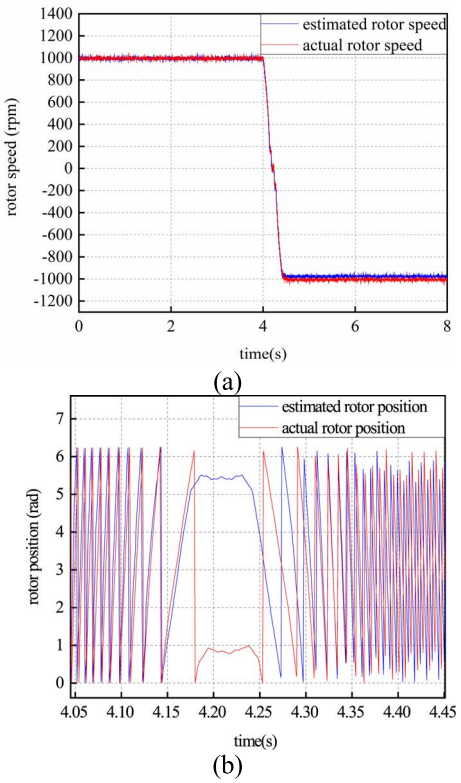

FIGURE 14. Experimental results of traditional SMO + traditional PLL when motor positive and negative speed switching. Rotor speed. (b) rotor position.

TABLE 4. Simulation results.

	Traditional SMO	Improved SMO
Maximum steady state error of speed	10 rpm	1 rpm
Maximum steady state error of rotor position	0.048 rad	0.021 rad

speed of the traditional SMO is 10 rpm and the maximum steady-state error of the rotor position is 0.048 rad. The maximum steady-state error of the rotational speed of the improved SMO is 1 rpm and the maximum steady-state error of rotor position is 0.021 rad. Therefore, the improved SMO can suppress chattering and reduce the speed and rotor position errors. The improved SMO has better observation performance. Fig. 9 shows the simulation results of the traditional SMO and the traditional PLL when the positive and negative speed of the motor is switched. Fig. 10 shows the simulation results of the improved SMO and tangent function PLL when the positive and negative speed of the motor is switched. The motor starts at no load and then runs at 1000 rpm. The speed is switched to −1000 rpm at 0.5 s. The simulation results show that the traditional PLL can not be used for the positive and negative speed switching of motor. The tangent function PLL can realize the observation of rotor speed and rotor position under the condition of positive and negative speed switching.

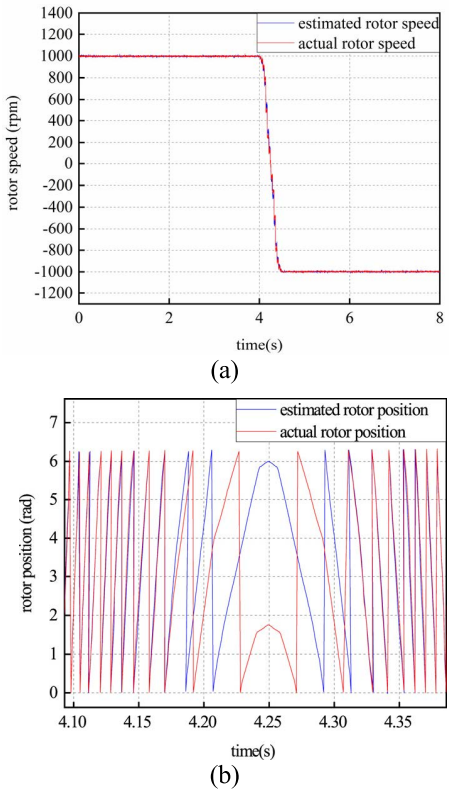

FIGURE 15. Experimental results of improved SMO + tangent function PLL during positive and negative speed switching of motor. (a) Rotor speed. (b) rotor position.

V. EXPERIMENTAL VERIFICATION

In order to further verify the feasibility of the sensorless control method of PMSM proposed in this paper, the experimental research is carried out on the 2 kW surface mounted PMSM vector control platform with TMS320F28335 as the main control chip. Fig. 11 shows the experimental platform, which is mainly composed of test motor, load motor, host computer, speed and torque sensor, data acquisition card, DC power supply and power drive module. The test motor used in the experiment is driven by TMS320F28335 chip of TI company to realize the sensorless control algorithm. The load motor is powered by industrial inverter to provide the load required for the experiment. The speed torque sensor is connected between the two motors using a coupling. The sensor data is collected to the upper computer by the acquisition card, the current and voltage are measured by 12 bit A/D converter. The parameters of PMSM used in the experiment are the same as those of simulation, as shown in Table 3. The experiment and simulation are carried out under the same conditions. The switching frequency is 10 kHz and the sampling period is 50 μs.

Fig. 12 shows the experimental results of a conventional SMO. Fig. 13 shows the experimental results of the improved SMO. Table 5 shows the comparison of the experimental results of the two control methods. The experiment and simulation are carried out under the same conditions. The experimental results show that the improved SMO can effectively suppress chattering and reduce rotor speed and rotor position errors. Fig. 14 shows the experimental results of the traditional SMO and the traditional PLL. Fig. 15 shows the experimental results of the improved SMO and tangent function PLL. As can be seen from the figure, compared with the traditional PLL, the tangent function PLL can still accurately estimate the rotor speed and rotor position under the condition of positive and negative speed switching. The same results are obtained by experiment and simulation to verify the effectiveness and feasibility of the proposed algorithm.

TABLE 5. Experimental results.

	Traditional SMO	Improved SMO
Maximum steady state error of speed	35 rpm	8.6 rpm
Maximum steady state error of rotor position	0.156 rad	0.078 rad

VI. CONCLUSION

Aiming at the problems of low observation accuracy and serious chattering of traditional SMO, a sensorless control scheme of PMSM based on FSMO is proposed in this paper. In order to reduce chattering, sigmoid function is used instead of sign function as switching function. Fuzzy rules are established to adaptively adjust the parameter a in sigmoid function according to the actual operation of the system. The value of a will affect the convergence speed of sigmoid function. By adaptively adjusting the value of a, we can ensure faster convergence speed and less chattering of the system. The back EMF adaptive law is used to smooth the back EMF signal to reduce the observation error and improve the observation accuracy. In addition, a tangent function PLL is proposed to solve the problem that the traditional PLL can not observe the rotor speed and rotor position under the condition of positive and negative speed switching. The tangent function is used to avoid the value and symbol of back EMF entering the system, so as to realize accurate observation during positive and negative speed switching. The effectiveness and feasibility of the designed method are verified by simulation and experiment.

CONFLICT OF INTEREST

The authors declare no conflict of interest, financial or otherwise.

REFERENCES

[1] X. Wu, Z. Lv, Z. Ling, X. Zhang, and G. Tan, "An improved pulse voltage injection based initial rotor position estimation method for PMSM," *IEEE Access*, vol. 9, pp. 121906–121915, 2021.

[2] G. Wang, J. Kuang, N. Zhao, G. Zhang, and D. Xu, "Rotor position estimation of PMSM in low-speed region and standstill using zero-voltage vector injection," *IEEE Trans. Power Electron.*, vol. 33, no. 9, pp. 7948–7958, Sep. 2018.

[3] D. S. Nair, G. Jagadanand, and S. George, "Torque estimation using Kalman filter and extended Kalman filter algorithms for a sensorless direct torque controlled BLDC motor drive: A comparative study," *J. Electr. Eng. Technol.*, vol. 16, no. 5, pp. 2621–2634, Jun. 2021.

[4] A. Gundogdu, R. Celikel, and O. Aydogmus, "Comparison of Si-ANN and extended Kalman filter-based sensorless speed controls of a DC motor," *Arabian J. Sci. Eng.*, vol. 46, no. 2, pp. 1241–1256, Feb. 2021.
[5] J. She, L. Wu, C.-K. Zhang, Z.-T. Liu, and Y. Xiong, "Identification of moment of inertia for PMSM using improved modelreference adaptive system," *Int. J. Control, Autom. Syst.*, vol. 20, no. 1, pp. 13–23, Jan. 2022.
[6] E. Ojionuka, I. Chinaeke-Ogbuka, C. Ogbuka, and C. Nwosu, "A simplified sensorless speed control of permanent magnet synchronous motor using model reference adaptive system," *J. Electr. Eng.*, vol. 70, no. 6, pp. 473–479, Dec. 2019.
[7] X. Sun, Y. Zhang, X. Tian, J. Cao, and J. Zhu, "Speed sensorless control for IPMSMs using a modified MRAS with gray wolf optimization algorithm," *IEEE Trans. Transp. Electrific.*, vol. 8, no. 1, pp. 1326–1337, Mar. 2022.
[8] X. Sun, T. Li, Z. Zhu, G. Lei, Y. Guo, and J. Zhu, "Speed sensorless model predictive current control based on finite position set for PMSHM drives," *IEEE Trans. Transp. Electrific.*, vol. 7, no. 4, pp. 2743–2752, Dec. 2021.
[9] W. Xu, S. Qu, L. Zhao, and H. Zhang, "An improved adaptive sliding mode observer for middle- and high-speed rotor tracking," *IEEE Trans. Power Electron.*, vol. 36, no. 1, pp. 1043–1053, Jan. 2021.
[10] Z. Qiao, T. Shi, Y. Wang, Y. Yan, C. Xia, and X. He, "New sliding-mode observer for position sensorless control of permanent-magnet synchronous motor," *IEEE Trans. Ind. Electron.*, vol. 60, no. 2, pp. 710–719, Feb. 2013.
[11] H. Kim, J. Son, and J. Lee, "A high-speed sliding-mode observer for the sensorless speed control of a PMSM," *IEEE Trans. Ind. Electron.*, vol. 58, no. 9, pp. 4069–4077, Sep. 2011.
[12] J. Xiong and H. Gu, "Research on a sliding mode variable structure control FOC of PMSM for electric vehicles," in *Proc. IEEE 9th Int. Conf. Softw. Eng. Service Sci. (ICSESS)*, Beijing, China, Nov. 2018, pp. 1088–1091.
[13] S. Singh and S. Lee, "Design of integral sliding mode control using decoupled disturbance compensator with mismatched disturbances," *Int. J. Control, Autom. Syst.*, vol. 19, no. 10, pp. 3264–3272, Oct. 2021.
[14] G. Wang and H. Zhang, "A new speed adaptive estimation method based on an improved flux sliding-mode observer for the sensorless control of PMSM drives," *ISA Trans.*, vol. 15, no. 8, pp. 1553–1562, Sep. 2021.
[15] B. Wang, Y. Shao, Y. Yu, Q. Dong, Z. Yun, and D. Xu, "High-order terminal sliding-mode observer for chattering suppression and finite-time convergence in sensorless SPMSM drives," *IEEE Trans. Power Electron.*, vol. 36, no. 10, pp. 11910–11920, Oct. 2021.
[16] C. H. Jiang, Q. M. Wang, Z. H. Li, N. N. Zhang, and H. T. Ding, "Nonsingular terminal sliding mode control of PMSM based on improved exponential reaching law," *Electronics*, vol. 10, no. 15, p. 1776, Aug. 2021.
[17] W. Xu, A. K. Junejo, Y. Liu, M. G. Hussien, and J. Zhu, "An efficient antidisturbance sliding-mode speed control method for PMSM drive systems," *IEEE Trans. Power Electron.*, vol. 36, no. 6, pp. 6879–6891, Jun. 2021.
[18] D. Ke, F. Wang, L. He, and Z. Li, "Predictive current control for PMSM systems using extended sliding mode observer with hurwitz-based power reaching law," *IEEE Trans. Power Electron.*, vol. 36, no. 6, pp. 7223–7232, Jun. 2021.
[19] A. T. Woldegiorgis, X. Ge, H. Wang, and M. Hassan, "A new frequency adaptive second-order disturbance observer for sensorless vector control of interior permanent magnet synchronous motor," *IEEE Trans. Ind. Electron.*, vol. 68, no. 12, pp. 11847–11857, Dec. 2021.
[20] S. Wu, J. Zhang, and B. Chai, "Adaptive super-twisting sliding mode observer based robust backstepping sensorless speed control for IPMSM," *ISA Trans.*, vol. 92, pp. 155–165, Sep. 2019.
[21] L. Wenqi, H. Yuwen, H. Wenxin, C. Jianbo, D. Xuyang, and Y. Jianfei, "Sensorless control of permanent magnet synchronous machine based on a novel sliding mode observer," in *Proc. IEEE Vehicle Power Propuls. Conf.*, Sep. 2008, pp. 1–4.
[22] L. Sheng, W. Li, Y. Wang, M. Fan, and X. Yang, "Sensorless control of a shearer short-range cutting interior permanent magnet synchronous motor based on a new sliding mode observer," *IEEE Access*, vol. 5, pp. 18439–18450, 2017.
[23] R. Li and Y. Yang, "Sliding-mode observer-based fault reconstruction for T-S fuzzy descriptor systems," *IEEE Trans. Syst., Man, Cybern., Syst.*, vol. 51, no. 8, pp. 5046–5055, Aug. 2021.
[24] Y. C. Dai, S. F. Ni, D. Z. Xu, L. Y. Zhang, and X. G. Yan, "Disturbance-observer based prescribed-performance fuzzy sliding mode control for PMSM in electric vehicles," *Eng. Appl. Artif. Intell.*, vol. 104, Sep. 2021, Art. no. 104361.
[25] Y. Zhang, Y. Nie, and L. Chen, "Adaptive fuzzy fault-tolerant control against time-varying faults via a new sliding mode observer method," *Symmetry*, vol. 13, no. 9, p. 1615, Sep. 2021.
[26] B. Kelkoul and A. Boumediene, "Stability analysis and study between classical sliding mode control (SMC) and super twisting algorithm (STA) for doubly fed induction generator (DFIG) under wind turbine," *Energy*, vol. 214, Jan. 2021, Art. no. 118871.
[27] X. Xiong, R. Kikuuwe, S. Kamal, and S. Jin, "Implicit-euler implementation of super-twisting observer and twisting controller for second-order systems," *IEEE Trans. Circuits Syst. II, Exp. Briefs*, vol. 67, no. 11, pp. 2607–2611, Nov. 2020.
[28] D. Liang, J. Li, R. Qu, and W. Kong, "Adaptive second-order sliding-mode observer for PMSM sensorless control considering VSI nonlinearity," *IEEE Trans. Power Electron.*, vol. 33, no. 10, pp. 8994–9004, Oct. 2018.
[29] Y.-C. Liu, S. Laghrouche, A. N'Diaye, and M. Cirrincione, "Hermite neural network-based second-order sliding-mode control of synchronous reluctance motor drive systems," *J. Franklin Inst.*, vol. 358, no. 1, pp. 400–427, Jan. 2021.
[30] J. Guo, K. Li, J. Fan, Y. Luo, and J. Wang, "Neural-fuzzy-based adaptive sliding mode automatic steering control of vision-based unmanned electric vehicles," *Chin. J. Mech. Eng.*, vol. 34, no. 1, p. 88, Dec. 2021.
[31] X. Sun, J. Cao, G. Lei, Y. Guo, and J. Zhu, "A composite sliding mode control for SPMSM drives based on a new hybrid reaching law with disturbance compensation," *IEEE Trans. Transp. Electrific.*, vol. 7, no. 3, pp. 1427–1436, Sep. 2021.
[32] C. Olivieri and M. Tursini, "A novel PLL scheme for a sensorless PMSM drive overcoming common speed reversal problems," in *Proc. Int. Symp. Power Electron. Power Electron., Electr. Drives, Autom. Motion*, Jun. 2012, pp. 1051–1056.
[33] S. Lin and W. Zhang, "An adaptive sliding-mode observer with a tangent function-based PLL structure for position sensorless PMSM drives," *Int. J. Elect. Power Energy Syst.*, vol. 88, pp. 63–74, Jun. 2017.

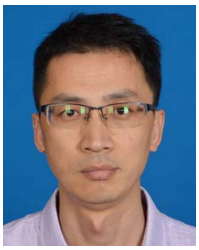

HONGCHANG DING received the bachelor's, master's, and Ph.D. degrees from the Shandong University of Science and Technology. He is currently an Associate Professor with the Department of Energy and Power Engineering, College of Mechanical and Electronic Engineering, Shandong University of Science and Technology. His research interests include sensorless control of high-speed permanent magnet synchronous motor, CFD numerical simulation of internal flow field of centrifugal pump, and performance optimization.

XINHONG ZOU received the bachelor's degree from the Shandong University of Science and Technology, where he is currently pursuing the master's degree with the College of Mechanical and Electronic Engineering. His research interest includes the sensorless control of high-speed permanent magnet synchronous motor.

JINHONG LI received the bachelor's degree from the Taishan College of Science and Technology, Shandong University of Science and Technology, where he is currently pursuing the master's degree with the College of Mechanical and Electronic Engineering. His research interest includes the sensorless control of high-speed permanent magnet synchronous motor.